Low-power supralinear photocurrent generation via excited state fusion in single-component nanostructured organic photodetectors

Low-Power Non-linear Photocurrent Generation via Excited State Fusion in Single-component Nanostructured Organic Photodetectors

Giannis Antoniou [a)], Peisen Yuan [a)], Loukas Koutsokeras [a)], Stavros Athanassopoulos [b)], Daniele Fazzi [c)], Julianna Panidi [d)], Dimitra G. Georgiadou [d)], Themis Prodromakis [d)], Panagiotis E. Keivanidis [a)]*

a) Device Technology and Chemical Physics Laboratory, Department of Mechanical Engineering and Materials Science and Engineering, Cyprus University of Technology, 45 Kitiou Kyprianou str., Limassol 3041, Cyprus

b) Departamento de Fisica, Universidad Carlos III de Madrid, Spain

c) Dipartimento di Chimica "Giacomo Ciamician", Università di Bologna, via F. Selmi 2, 40126, Bologna (Italy)

d) Centre for Electronics Frontiers, Electronics and Computer Science, University of Southampton, Highfield Campus, University Road, Building 53 (Mountbatten), Southampton SO17 1BJ, United Kingdom

AUTHOR INFORMATION

Corresponding Author

* Panagiotis E. Keivanidis

The integration of triplet-triplet annihilation (TTA) components as electrically and optically active elements in vertically-configured photoactive device architectures is a challenging task to achieve. Herein we present a simple methodology for incorporating a photon absorbing layer of the (2,3,7,8,12,13,17,18-octaethyl-porphyrinato) Pt^{II} (PtOEP) metallorganic complex, as a self-TTA annihilator medium in a sandwich-like photodiode device structure. At low power illumination, the PtOEP photodiode exhibits photocurrent generation via the fusion of optically induced PtOEP excited states and it develops an open-circuit voltage (V_{OC}) as high as 1.15 V. The structural and the spectroscopic characterization of the nanostructured PtOEP photoactive layer in combination with density functional theory calculations identify PtOEP dimer species as the annihilating excited state responsible for the formation of charges. The participation of the fusion process in the mechanism of charge photogeneration manifests in the quadratic dependence of the short-circuit current density (J_{SC}) on the incoming photoexcitation intensity, both when incoherent and coherent light is used for illuminating the PtOEP diodes. The non-linear photoresponse of the PtOEP device allows for the highly selective and sensitive photodetection within the 500 - 560 nm narrow spectral range. At short-circuit conditions a power-law is observed on the dependence of the device responsivity on fluence.

ey

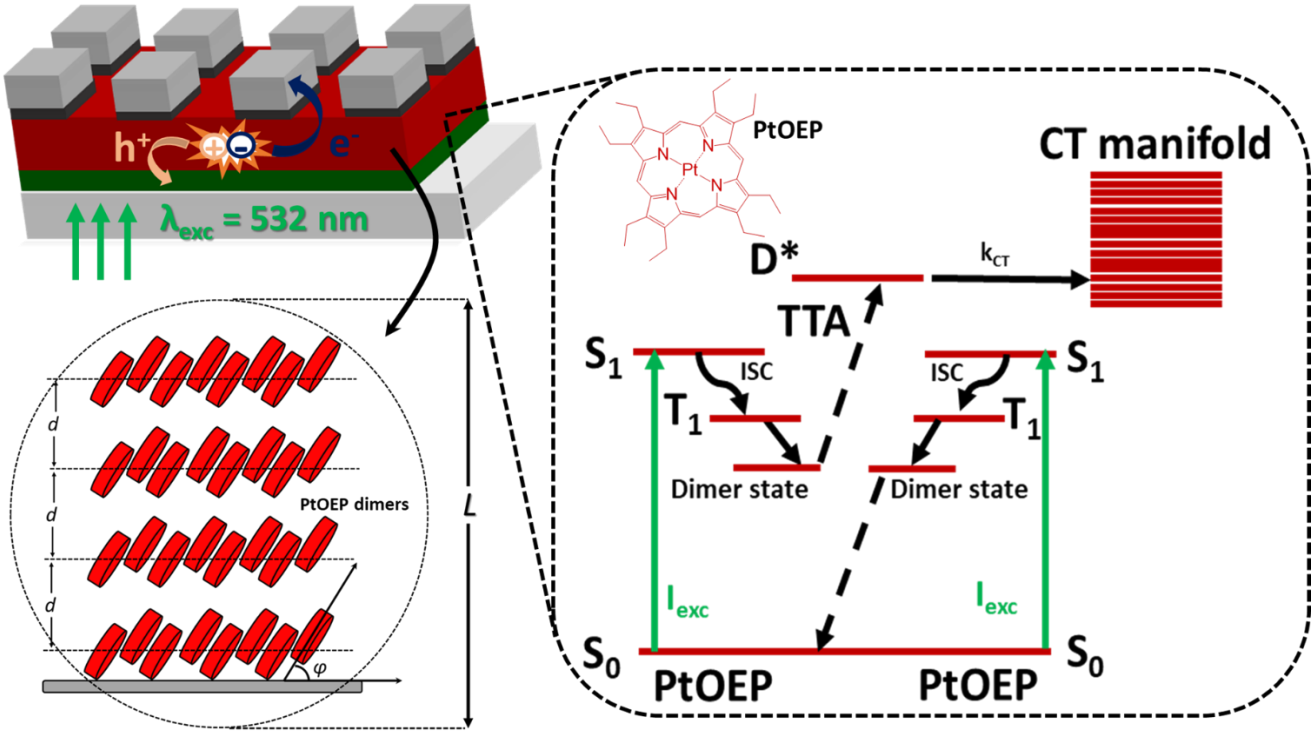

TOC GRAPHICS

KEYWORDS Smart light management, energy pooling, solar cells, singlet fission, subgap photon absorption, spin-entangled pair states

Organic semiconductor materials represent a leading class of next generation molecular systems that have revolutionized the field of optoelectronic devices and have established a range of transforming technologies such as light emitting diodes, [1], [2] field effect transistors (FETs), [3], solar cells [4] and photodetecting devices. [5] Since the advent of molecular crystals, the formation of carriers by light absorption in π-conjugated organic materials has been the topic of intensive research. [6]Small-molecule and polymeric material structures containing sp^2-hybridized carbon atoms exhibit high absorption coefficients thereby undergoing highly allowed electronic transitions via one-photon absorption steps that result in the formation of excitonic states.

Especially for the case of vertically-configured photoactive device architectures that aim to light detection i.e. organic photodetecting devices (OPDs), charge photogeneration is of paramount importance to their performance level. Like in the case of organic solar cell devices, the exciton state in OPDs serves as a precursor of charge transfer (CT) states that facilitate charge photogeneration. [7], [8] Owing to the relatively high exciton binding energy in organic semiconductors, exciton dissociation is rarely spontaneous and it is achieved with the aid of a driving force that facilitates the activation of CT states. CT state activation is typically achieved by the formation of heterojunctions between the photoexcited organic material and another material that is either in the form of unwanted impurities [9] or deliberately placed species capable to accept an electron (hole) from the LUMO (HOMO) level of the photoexcited organic material. [10] In the absence of heterojunctions, intrinsic charge photogeneration is inefficient and may occur by i) the compensation of the exciton binding energy with the application of an external electric field [9], [11] ii) offsets in the electrostatic potential in the photoactive layer due to the different structural organization of the organic material [12], or iii) non-linear light absorption processes induced by two-photon or sequential photon absorption. [13]

During the last years one-photon absorption OPD platforms have demonstrated a remarkable progress. [14] [15], [16] [17] Irrespectively of the way charges are formed in OPDs, the main figures of merit to be considered are the device responsivity parameter (R), the dark current density (J_d), the noise-equivalent power (*NEP*) and the specific detectivity (D^*) parameters. The R parameter corresponds to the ratio of the registered photocurrent in respect to the incident light intensity [18], [19]. The *NEP* parameter represents the lowest incident light power at which no discernible output signal photocurrent can be obtained in respect to the noise current [16], [20], [21] whereas D^* describes the ability of the photodetector to respond to low level incident light power, independently of the device photoactive area. [22], [23]. Recent reports have presented high-performing bulk heterojunction donor/acceptor OPD layers of subphthalocyanine derivatives [24] that exhibit low J_d and high R values in the order of 53.1 nA cm^{-2} and 250 mA W^{-1}, respectively. Fullerene-free OPDs deliver state-of-the-art *NEP* values of 0.22 × pW $Hz^{-1/2}$ under 532 nm illumination [25] and D^* values as high as 3.3×10^{11} Jones at 560 nm photoexcitation. [20] Further progress is noted recently by covalently linking the donor and the acceptor components of the OPD layer in order to achieve a single component OPD photoactive layer. [26] For these OPDs the detection of 633 nm light with intensity of 500 μW cm^{-2} was achieved with an R of 0.9 mA W^{-1} while D^* was ~ 2×10^9 Jones.

Contrary to the cases of one-photon absorption devices, not much attention has been paid to OPDs that exhibit non-linear photocurrent generation via multiphoton absorption schemes. This lack of progress is attributed mainly to the complex technicalities that require the use of ultrashort *i.e.* fs and high repetition laser pulses to establish the proper conditions that facilitate the two-photon or sequential photon absorption transitions. Nevertheless, the technological significance of non-linear photodetectors has been recognized. [27] An alternative approach for

realizing non-linear OPDs without necessarily employing high-power ultrafast pulsed laser sources would be the utilization of excited state fusion reactions that in principle can support the activation of CT states [28], [29], [30].

In this work we set out to explore the possibility to enable photocurrent generation via the fusion of long-lived excited states in photodiodes of the (2,3,7,8,12,13,17,18-octaethyl-porphyrinato) platinum (II) (PtOEP) phosphorescent dye; a disk-shaped metallo-organic complex that is a well-established triplet-emitter in organic electronics. [31] The long-lived triplet excited state of PtOEP offers the opportunity to achieve a non-linear photoresponse by employing less demanding optical photoexcitation schemes *i.e.* incoherent light sources or low-power, continuous-wave (cw) monochromatic laser photoexcitation. For our work we focus on a vertically-configured OPD device platform with a thermally evaporated PtOEP photoactive layer. The absorption spectrum of PtOEP layer lies within the visible spectral range; its absorption edge is located at about 640 nm and it is attributed to the $S_0 - T_1$ transition. By photoexciting the PtOEP complex at lower wavelengths (500 – 600 nm, Q-band) the first singlet excited (S_1) state is populated. [32], [33] In presence of the Pt heavy atom, the efficient spin–orbit coupling (SOC) between the singlet and triplet manifolds facilitates the fast intersystem-crossing (ISC) to the triplet excited state (T_1) from where phosphorescence is generated. Based on the peak intensity of the characteristic PtOEP phosphorescence, the energy of the first triplet excited level is placed at 1.9 eV. In addition, PtOEP possesses a deep highest occupied molecular orbital (HOMO) level that is energetically placed at -5.3 eV [34], [35], thereby making PtOEP suitable to facilitate hole extraction at the hole-collecting electrode of a photodiode device structure. Owing to its long-lived triplet excited state, PtOEP has the capability to undergo triplet-triplet annihilation (TTA) reactions and to store photon energy in a TTA-mediated higher lying PtOEP state. [36] [37] [38] [39] [40] It is therefore

meaningful to consider PtOEP as an ideal material for establishing TTA-driven charge photogeneration. Being electronically coupled in a photodiode configuration, PtOEP can undertake simultaneously the roles of photon absorbing, TTA annihilating, charge generating and charge transporting material. Concerning charge transport, p-channel organic FETs with epitaxially grown PtOEP layers have been demonstrated where hole mobility was found to be as high as μ_{FET} = 2.2 $\times 10^{-4}$ cm^2 $V^{-1}s^{-1}$. [41] In disk-shaped metallo-porphyrin complexes charge transport takes place along the π-π stacking direction of the porphyrin macrocycles. While in amorphous metallo-porphyrin films hole mobility is limited by trapping sites [42], the development of well-structured porphyrin assemblies [43] can improve stacking along the π-π direction. Earlier studies have proposed the use of porphyrin complexes for charge photogeneration via triplet exciton dissociation. [44] In regard to photoconductivity, the propensity of PtOEP films to produce charges after photoexcitation has been studied in symmetric photodiodes, equipped with semitransparent aluminum (Al) electrodes. [45] In those systems, photoconductivity in PtOEP was monitored in ambient atmosphere and at room temperature after exciting the PtOEP photodiodes with incoherent light, while applying an electric field of 1.5 $\times 10^5$ V cm^{-1}. Photoconductivity in PtOEP devices was attributed to the dissociation of PtOEP triplet excitons that proceeds according to the Onsager theory of geminate charge recombination. [10] The short-circuit current density of those photodiodes was found to follow a linear-to-square root dependence on light fluence, and the observed transition was understood as the outcome of photocurrent losses due to bimolecular charge recombination when fluence exceeded the threshold of 10^{14} $cm^{-2}s^{-1}$.

In our present work we demonstrate the capability of PtOEP photodiodes to support non-linear photocurrent generation vie excited state fusion that manifests in the quadratic dependence of photocurrent density on photoexcitation. When a 532 nm cw-laser source is used the obtained J_{SC}

and V_{OC} of the PtOEP-photodiodes become as high as 0.24 mA cm^{-2} and 1.15 V, respectively. Our work demonstrates a generic scheme of how triplet exciton annihilators can be employed as optically and electrically integrated interlayers to sensitize vertically-configured OPD and OSC device platforms via TTA reactions.

Figure 1a presents the chemical structure of PtOEP, together with the frontier level alignment of the metallo-porphyrin in respect to the work function of the device electrodes. As shown in Figure 1b, the typical external quantum efficiency (EQE) spectrum of the PtOEP photodiode confirms the responsivity to incoming light. A clear photo-response is observed albeit the photocurrent generation efficiency of the system remains very low. In the obtained EQE spectra, two spectral features are clearly discernable at 3.26 eV (380 nm) and at 2.25 eV (550 nm) with EQEs in the order of 0.10%. Direct comparison with the absorption spectrum of PtOEP in dilute solution points to the origin of the EQE features. The photocurrent peak detected at about 2.25 eV corresponds to onset of the Q-band in the absorption spectrum of PtOEP, thereby suggesting that charge photogeneration is barrierless. The high energy photocurrent peak is attributed to transitions within the Soret absorption band of PtOEP. In respect to the UV-Vis absorption spectra in solution, both EQE features of PtOEP are spectrally broadened. Moreover, the full-width half maximum (FWHM) value of the photocurrent peak at 550 nm is increased in respect to the FWHM value of the Q-absorption band. The low efficiency with which carriers are photogenerated in the PtOEP photodiode should not be surprising given the absence of a heterojunction in the photoactive layer that could drive exciton dissociation via charge transfer. One could argue that by considering the PtOEP layer thickness (120 nm) and the asymmetric electrodes used in the PtOEP-photodiode, the observed photocurrent originates from the portion of weakly bound PtOEP excitons that are fully separated by the build-in electric field of the

photodiode device. Given the relatively high dielectric constant of PtOEP (ε=12) [46], the dissociation of the PtOEP excitons is likely facilitated by the well-ordered fraction of the thermally evaporated layer.

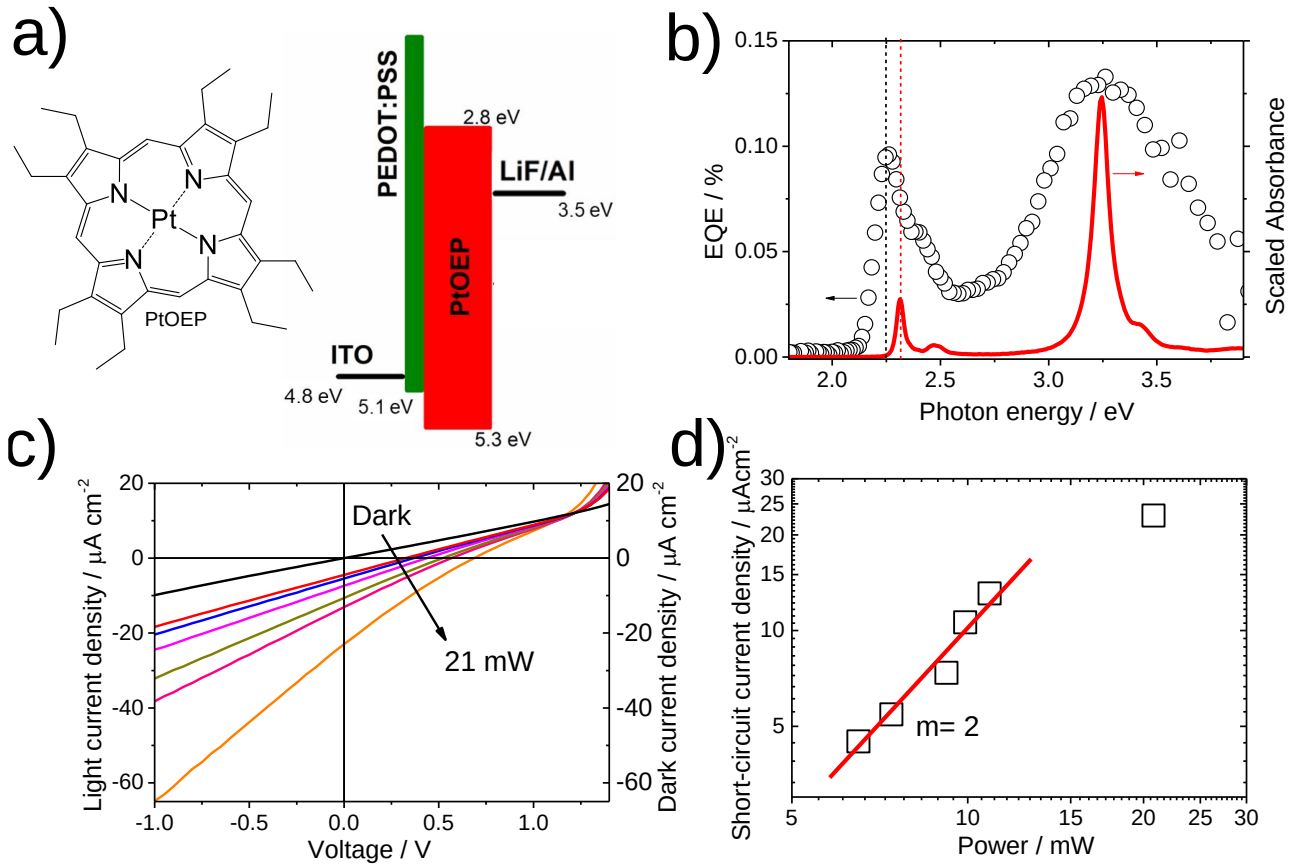

Figure 1: a) Chemical structure of PtOEP, energy levels of the materials and electrodes work function. b) the external quantum efficiency spectrum of a PtOEP device and the scaled absorption spectrum of a PtOEP solution in toluene, c) J-V curves under dark and light conditions and d) the dependence of device J_{SC} on the power of white light used to illuminate the diodes.

We have further recorded the J-V characteristics of the PtOEP photodiodes under white light illumination, as provided by a Hg/Xe arc lamp. Figure 1c presents the obtained light J-V curves of the PtOEP diode at different incoming light power, together with the dark J-V characteristics of the device. For an illumination power of 21 mW, the open-circuit voltage (V_{OC}) and the short-circuit current density (J_{SC}) of the device become $V_{OC} \sim 0.6$ V and $J_{SC} \sim 23$ μA cm^{-2}. Unlike previous results of studies on the photoconductivity of porphyrin-based materials [45], [47], Figure 1d shows that the device J_{SC} exhibits a quadratic dependence on the incoming light power. Considering the incoherent nature of light used for photoexciting the PtOEP device, this observation is rather surprising as it suggests the participation of a non-linear process [13] in the mechanism of charge photogeneration in the PtOEP device system.

In order to gain solid insight on the observed photocurrent dependence on light power we first addressed the structural properties of the PtOEP photoactive layer. Figure 2a presents the X-ray diffractogram (XRD) of a thermally evaporated PtOEP film on a quartz substrate. For reference purposes, XRD patterns are presented for PtOEP in the powder form and for a solution-processed PtOEP film. The latter was obtained by spin coating of a PtOEP solution in toluene in which PtOEP was mixed (10 wt%) with a high molecular weight atactic-poly(styrene) (a-PS) derivative.

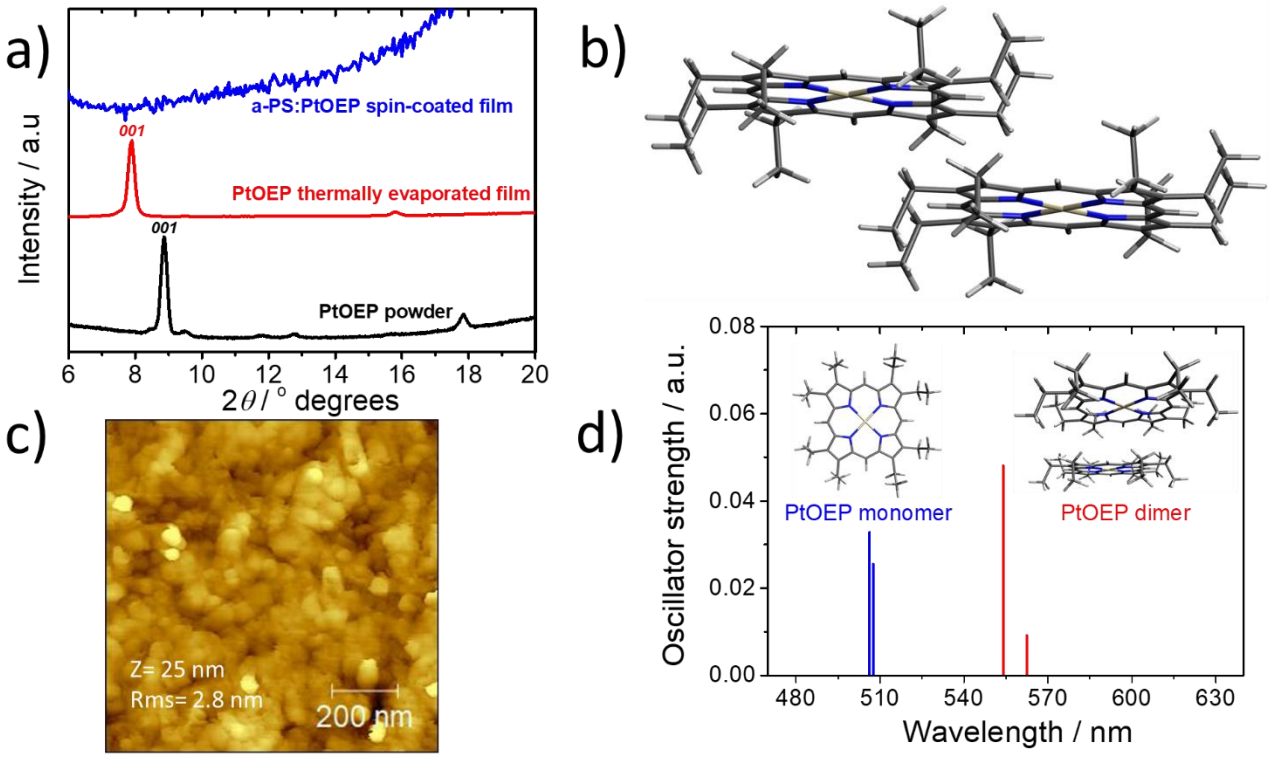

Figure 2. a) XRD patterns of the PtOEP system in the form of powder (black line), a thermally evaporated film (red line) and a spin-coated a-PS:PtOEP film (blue line). b) Tapping mode AFM image of the evaporated PtOEP film on glass/ITO/PEDOT:PSS. c) DFT calculated side-view of the PtOEP dimer configuration, and d) oscillator strength for PtOEP monomer (blue) and dimer (red).

As shown in Figure 2a, the solution processed a-PS:PtOEP film is found to be amorphous. In contrast, the XRD pattern obtained for the thermally evaporated PtOEP film indicates the presence of PtOEP crystalline features that confirm the contribution of PtOEP structural order in photocurrent generation. With respect to the angular position of the (001) planes of PtOEP in the powder form PtOEP (2θ= 8.86°), the observed diffraction peak of the evaporated PtOEP film is placed at 2θ= 7.87°, indicating a periodicity of d= 11.2 Å. Control measurements on a similarly

prepared PtOEP film evaporated on a glass/ITO/PEDOT:PSS electrode exhibited an identical XRD (not shown) without differences in the angular position of the PtOEP (001) planes. The derived periodicity of 11.2 Å is attributed to the intercolumnar distance between PtOEP columns in the layer that adapt an edge-on orientation on the quartz substrate. [48] Based on the FWHM of the (001) diffraction peak the calculated coherence length of the PtOEP crystallite is L= 40 nm. We further applied atomic force microscopy (AFM) imaging for the mapping the surface topography of the evaporated PtOEP film on glass/ITO/PEDOT:PSS substrate. As shown in Figure 2b the surface of the film is found relatively smooth with a root mean square roughness (Rms) of 2.8 nm. In good agreement with the obtained XRD characterization results, the topography mapping verifies the formation of PtOEP crystallites on the PtOEP film surface with an average size of 50 nm.

Both XRD and AFM studies provide evidence in support the semicrystalline character of the thermally evaporated PtOEP film. For investigating the exciton coupling effects between the PtOEP molecules in the crystalline fraction of the film and for addressing their impact on the absorption properties of the PtOEP system, density functional theory (DFT) calculations were performed on isolated (*i.e.* monomer) and aggregated (*i.e.* dimer) PtOEP species. The aggregation of PtOEP was studied based on constraint optimizations of the PtOEP dimer wherein the interatomic Pt – Pt distance of the two π-π stacked PtOEP molecules was kept fixed to 8.165 Å, as obtained from the packing motif of the PtOEP single crystal. [49]. In these calculations the ethyl side groups of the PtOEP macrocycle were explicitly considered. According to the DFT results the interaction of two PtOEP monomers affects the PtOEP Q-band spectral characteristics. As shown in Figure 2d, the low energy transitions found at 506 and 507 nm for

the PtOEP monomer split and exhibit a red-shift to 554 nm and 562 nm for the constrained PtOEP dimer.

As a next step, the UV-Vis absorption spectra of the thermally evaporated PtOEP film were measured. For reference purposes, the UV-Vis spectra of the spin-coated a-PS:PtOEP film were also recorded. Figure 3a and Figure 3b present the normalized absorption spectra of these films in the range 450 – 600 nm where the Q-band of the PtOEP film is positioned. The spectrum of the spin-coated a-PS:PtOEP is found similar to that of PtOEP in dilute solution (see Fig. 1b), exhibiting absorption peaks of the Q-bands at 503 nm and 536 nm. In contrast, the absorption spectrum of the thermally evaporated film is found distorted; the Q-bands are broadened and red-shifted, while a shoulder appears in the absorption band between 540 – 550 nm (Supporting Information section). In light of the DFT findings, the splitting of the low energy Q-band is attributed to the onset of PtOEP dimer species formation in the thermally evaporated PtOEP film.

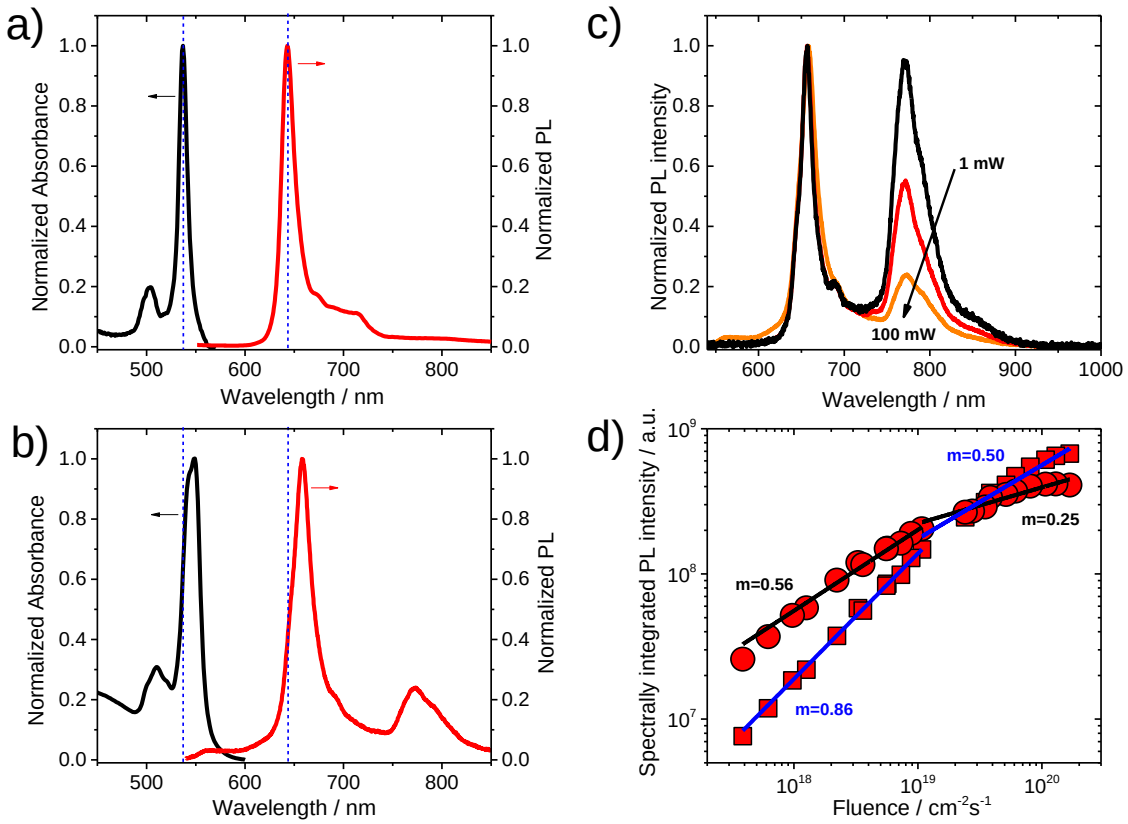

Figure 3. Normalized absorption (black line) and photoluminescence (red line) spectra of the a) spin-coated a-PS:PtOEP film and b) thermally evaporated PtOEP film. c) Normalized photoluminescence spectra of the thermally evaporated PtOEP film, as acquired at different laser photoexcitation powers; 1 mW (black line), 10 mW (red line) and 100 mW (orange line). d) The dependence of the spectrally integrated PL signal of the PtOEP monomer between 650 – 655 nm (red squares) and the PtOEP dimer luminescence between 755 – 815 nm (red filled circles) on laser fluence. In all cases the data were acquired after cw laser photoexcitation at 532 nm.

Further evidence for the occurrence of intermolecular interactions comes from the comparison of the photoluminescence (PL) spectra of the spin-coated and thermally deposited PtOEP films, as obtained after photoexcitation at 532 nm. Comparing the PL spectra of the two systems, a red-

shift is found in the typical PtOEP phosphorescence band, from 644 nm (a-PS:PtOEP, Figure 3a) to 650 nm (thermally evaporated PtOEP film, Figure 3b). What's more, the characteristic signature of the triplet dimer PtOEP [50] is clearly detected in the PL spectrum of the thermally evaporated PtOEP film, positioned at 780 nm. Figure 3c presents the normalized PL spectra of the thermally evaporated film, as obtained after photoexcitation at 532 nm at progressively increased laser powers. As laser power increases from 1 mW to 100 mW, the relative PL intensity of the PtOEP triplet dimer diminishes by exhibiting a ratiometric relationship in regard to the phosphorescence intensity of the PtOEP monomer. The PL dependence of the two PtOEP spectral features on photoexcitation intensity was studied in more detail. Figure 3d presents the fluence dependent spectrally integrated PL intensity of the monomeric phosphorescence and of the triplet dimer emission signal. In the low fluence regime, the PL intensity of the PtOEP triplet dimer exhibits a square root dependence on fluence that suggests the occurrence of bimolecular annihilation events between the dimer species. Annihilation between CT states has been observed previously in other organic systems [51], and similarly the PtOEP system in the form of thermally evaporated films is prone to these effects. [52] At the same photoexcitation regime, the dependence of the PtOEP monomer phosphorescence is nearly linear, and only when fluences higher than 1×10^{19} cm^{-2} s^{-1} are used a sublinear dependence is observed that suggests the onset of TTA reactions between triplet PtOEP excitons. The different thresholds of fluence where TTA reactions become important for the PtOEP triplet exciton and the PtOEP triplet dimer relate to their diffusion coefficient. With respect to the triplet PtOEP excitons, the triplet PtOEP dimer species is more susceptible to bimolecular reactions due to its lower diffusion coefficient. [52] Interestingly, the annihilation effects between triplet PtOEP dimer species correlate with the generation of photocurrent in the PtOEP device. In order to understand deeper how the fusion

events between PtOEP triplet dimer photoexcited states impact the photo-response of the PtOEP photodiodes, J-V characteristics were recorded for a range of 532 nm laser photoexcitation intensities.

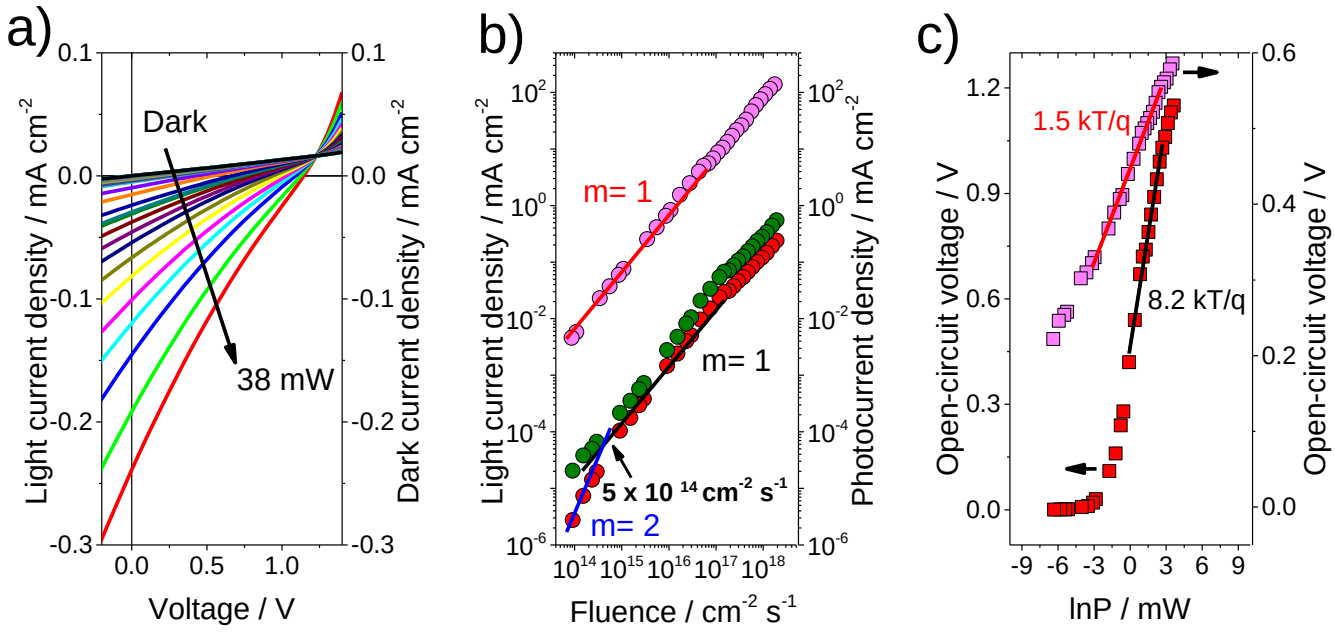

Figure 4. a) *J-V* curves of PtOEP device under 532 nm cw laser photoexcitation. b) PtOEP-photodiode short-circuit current density (red fill circles) and photocurrent density at -1 V (green fill circles) dependence on laser fluence. The dependence of a reference Si-based photodiode J_{SC} (magenta filled circles), on fluence is also displayed (guide to the eye slope lines). c) open-circuit voltage (V_{OC}) on the natural logarithm of excitation laser power (lnP) for the PtOEP-based (red filled squares) and Si-based (magenta filled squares) photodiodes.

The J-V curves acquired at different laser powers is presented in Fig. 4a, together with the corresponding dark J-V curve of the PtOEP-based device. From the data shown Fig. 4a the J_{SC} and V_{OC} parameters of the PtOEP device were derived for each laser power. The dependence of

J_{SC} on laser fluence and of V_{OC} on laser power are presented in Figure 4b and Figure 4c, respectively. For reference purposes, a commercially available Si-based photodetector was characterized under identical photoexcitation conditions and the excitation dependent J_{SC} and V_{OC} parameters are also presented. In good agreement with the quadratic dependence seen for the device J_{SC} under white light illumination (Fig. 1d), Fig.4b shows that the J_{SC} of the PtOEP device scales with the square of the incoming laser intensity at first while at higher fluences it gradually becomes linear. This square-to-linear transition is not observed in the case of the reference Si-based photodetector which exhibited a linear response across the entire fluence range used. When operating the PtOEP device at -1 V reverse bias, the dependence of photocurrent density J_{Ph} on fluence becomes linear for all fluences. In the presence of an externally applied electric field photogenerated charges become more mobile and have increased probability to participate in annihilation reactions with the PtOEP excited states. [53] Notably, at fluences higher than 5×10^{14} $cm^{-2}s^{-1}$ (~ 10 μW average laser power) both under -1 V reverse bias and at short-circuit conditions the device photocurrent exhibits a sublinear dependence on fluence that indicates the dominance of charge recombination losses. [10]

Turning attention to the impact of increasing photoexcitation intensity on V_{OC}, Figure 4c shows that V_{OC} gradually rises as laser power increases reaching to a plateau of 1.15 V. In principle, the dependence of V_{OC} on excitation intensity is expressed according to $V_{OC} = \beta \frac{kT}{q} \ln P$, where k corresponds to the Boltzmann constant, T to the absolute temperature, β to the thermal voltage ($\frac{kT}{q}$) coefficient, and P to the laser power. [54] By fitting the data of Figure 4c in this manner a thermal voltage coefficient value of β=8 is obtained that is well above the typical values between 1-2. [55] As shown in Fig.4c, the thermal voltage coefficient of the reference Si-photodiode is β=1.5 We presume that the performance of the PtOEP-only device is limited primarily by

nongeminate charge recombination losses due to the improper edge-on orientation arrangement of the disk-shaped PtOEP molecules on the device electrodes. This packing motif places the PtOEP π-π stacking direction vertically in respect to the required charge flow paths across the device electrodes. The structural defects that arise from this orthogonality impact negatively on the charge transport. Based on the dark J-V curves of unipolar hole-only PtOEP devices (see Figure S2 in Supporting Information), the zero-field electron hole (μ_h) mobility was determined to be $\mu_h = 3.7 \times 10^{-12}$ cm^2 V^{-1} s^{-1}.

Despite the non-optimized microstructure of the thermally evaporated PtOEP layer, the PtOEP-based photodiode offers an ideal opportunity to establish a platform for non-linear photocurrent generation with low photoexcitation power. Figure 5 presents the power-dependent values of the *R* device parameter. At -1 V reverse bias operation *R* is virtually independent on fluence, following the $R \propto \text{fluence}^{0.007}$ power-law. Practically it is found that *R* nests close to the level of 0.8 mA W^{-1} while the dark current density (J_d) is 13.2 μA cm^{-2}. In comparison with the state-of-the-art OPDs, the significantly weaker response of the herein presented PtOEP-based photodetector is not surprising considering that charge photogeneration is driven by the TTA-based mechanism. Contrary to the conventional route for charge photogeneration via the dissociation excitons formed by one-photon electronic transitions, the bimolecular nature of the TTA-driven charge generation mechanism in the single component PtOEP layer is less efficient. The applicability of the PtOEP system as a TTA-operated OPD unit was examined further by considering the *NEP* and D^* figures of merit. As presented in Table 1, the high J_d and low *R* values of the PtOEP photodetector concomitantly result in *NEP* and D^* values within 0.4 – 0.8 nW Hz$^{-1/2}$ and 3 - 6 × 10^8 Jones, respectively. Table 1 summarizes the values of these parameters

when operating the PtOEP- photodiode at the reverse bias of -1 V, under cw 532 nm laser illumination within the 1 μW - 3 mW regime of optical excitation.

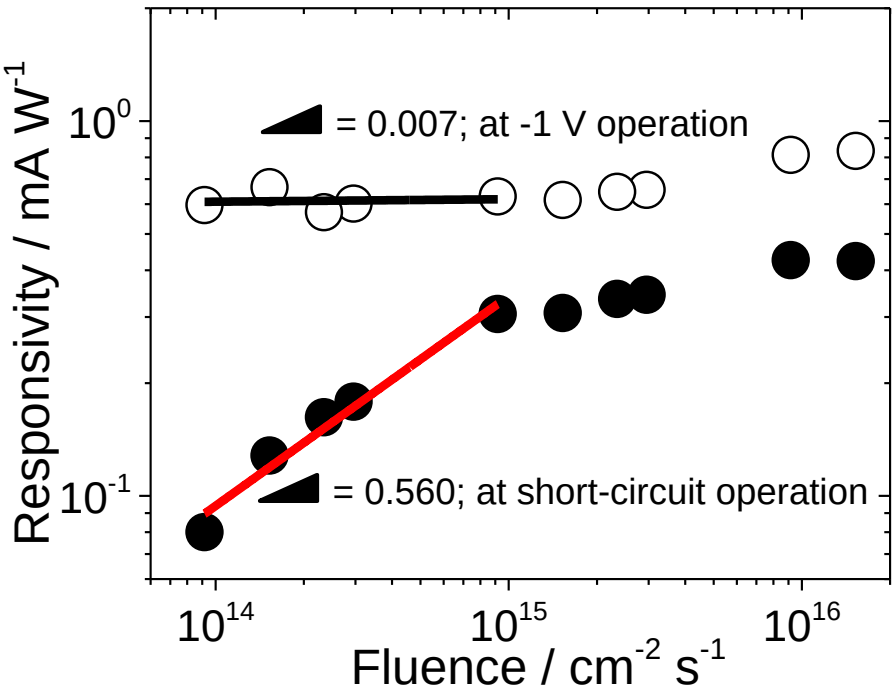

Figure 5. Fluence dependent responsivity of the PtOEP device when operating at short-circuit (filled symbols) and -1 V (open symbols) reverse bias conditions under illumination with a cw 532 nm laser. Dash lines correspond to power-law fits on the data.

Table 1: Optical power dependent values of the noise equivalent power (*NEP*) and specific detectivity (*D**) parameters for the PtOEP photodiode operated at -1 V under 532 nm cw-excitation.

Incident light power / µW	***NEP* / pW Hz$^{-1/2}$ [(a)]**	***D*** / Jones**
1.8	790	2.91×10^{8}
3	710	3.24×10^{8}
4.6	820	2.78×10^{8}
5.8	780	2.93×10^{8}
30	760	3.00×10^{8}
300	570	4.05×10^{8}
920	400	5.77×10^{8}
2910	390	5.92×10^{8}

[(a)] as measured at 1 Hz

The benefit of employing the non-linear photoresponse of the PtOEP photodiode in photodetection applications becomes clearer when operating the device at short-circuit. At this operation mode, in comparison with conventional OPDs, the PtOEP system offers the competitive advantage of high selectivity to low power optical stimulation signals. As shown in Figure 5, a gradual increase is observed in *R* for fluences below 10^{15} cm^{-2} s^{-1} and the power-law

dependence of $R \propto \text{fluence}^{0.560}$ is obtained; that is the PtOEP photodiode exhibits large differences in responsivity for minute differences in the incoming low-level photoexcitation intensity. At short-circuit conditions, J_d is vanishing and the detectivity of the PtOEP photodiode is inherently limited by thermal noise. [16] The highly selective and sensitive photodetecting response of the PtOEP photodiode within the 500 - 560 nm narrow spectral range is an attribute that can be utilized in next generation photonic and biophotonic applications. [27]

In summary, we studied the electro-optical properties of a single-component organic photodetector with a thermally evaporated PtOEP photoactive layer. Owing to the crystalline character of the PtOEP absorber, triplet dimer PtOEP species are formed in the layer that are prone to optically induced annihilation effects. With these structural characteristics, in addition to the role of light absorber, the PtOEP photoactive layer serves also as an electrically-integrated self-TTA activator and charge transporter in the device structure. The annihilation of triplet dimer PtOEP species in the layer of the PtOEP-only photodiode facilitates charge photogeneration and in combination with the deep HOMO level of PtOEP the development of an open circuit voltage as high as 1.2 V was achieved. The contribution of the bimolecular annihilation effects between triplet PtOEP dimers in the photoresponse of the device manifests in the quadratic dependence of the short-circuit current on photoexcitation intensity. The capability of PtOEP to activate photocurrent via self-TTA reactions is an added value to be utilized by a manifold of smart light-management photonic devices. A broad gamut of applications is envisioned including the use of TTA interlayers for sensitizing visible-blind photodetecting devices, stimulating neuromorphic and light-gated neural circuitries, and augmenting light-driven photocatalytic tandem platforms.

Experimental Methods

***Density functional theory calculations*:** The ground state equilibrium geometries of monomer and dimer PtOEP species were obtained using the dual-range local exchange-correlation functional M11-L and a mixed basis set, the triple-ζ Pople 6-311++G(d,p) basis set for C, H and N atoms and a Lanl2DZ basis with effective core potential for Pt. Vertical excited state energies were computed with linear response time dependent density functional theory (TD-DFT) on the basis of the optimized ground structures using the same functional and basis set.

***Materials*:** Atactic-poly(styrene) (a-PS, average M_w=192000 Da) was purchased from Sigma-Aldrich, poly(3,4-ethylenedioxythiophene) polystyrene sulfonate (PEDOT:PSS) was purchased from Merck (Clevios HTL Solar) and PtOEP was purchased from Frontier Scientific Inc. All materials were used as received without further purification.

Solution-processing and film development: Binary films of a-PS:PtOEP were deposited via spin coating of degassed solutions in toluene onto fused silica quartz substrates, in a nitrogen-filled glovebox.

***Deposition of PtOEP film and fabrication of PtOEP-only device*:** Thermally evaporated PtOEP films were deposited on fused silica substrates. Photodiode devices with thermally evaporated PtOEP active layers were developed based on the conventional device configuration of glass/indium tin oxide (ITO)/ PEDOT:PSS/PtOEP/lithium fluoride (LiF)/Aluminum (Al). The glass/ITO electrodes (XY15S, surface polished glass/indium tin oxide substrates from Xin Yan Technology Ltd.) were ultrasonically cleaned using acetone and isopropanol for 15 min. After preliminary cleaning, the substrates were washed with Hellmanex III to remove contaminants and residues from the ITO surface. The substrates were again cleaned with deionized water

followed by acetone and isopropanol for 15 min and soon after being placed in oxygen plasma (100 W power) for 10 min. A solution-processed hole-collecting interlayer of PEDOT:PSS was spin-coated at 3000 rpm for 1 min onto the ITO electrodes and thermal annealing was applied at 200 ºC for 20 minutes. The glass/ITO/PEDOT:PSS electrodes were transferred in a N_2-filled glovebox (PureLabHE, Inert) and a thermal evaporator (Covap III, Angstrom Engineering Inc.) coupled to the N_2-filled glovebox was used for depositing PtOEP in vacuum (4×10^{-8} mbar) at a rate of 0.5 Å/s. A shadow mask was used for facilitating the formation of a PtOEP layer area of 0.8 cm^2. The thickness of the obtained PtOEP film was 120 nm, as determined by a Tencor P16 Stylus profiler. The device structure was completed with the deposition of thermally evaporated LiF interlayer (~2 nm) at a rate of 0.1 Å/s capped by an Al (160 nm) metal electrode. A shadow mask facilitated the LiF interlayer and metal electrode deposition so that an effective device area of 0.0525 cm^2 was finally obtained. Prior to their removal from the glovebox the glass/ITO/PEDOT:PSS/PtOEP/LiF/Al photodiodes were encapsulated with glass slides and epoxy resin.

***UV-Vis absorption*:** The absorption spectra of the thermally evaporated PtOEP and the a-PS:PtOEP films were recorded with a UV-2700 Shimadzu spectrophotometer operated in transmission mode. In all cases, a spectral band width of 1 nm and a scan rate of 1 nm/s were used. For measuring the absorption spectra of the PtOEP solution in toluene, a cuvette of 10 mm path length was used and the obtained spectrum was corrected with respect to the absorption spectrum of pure toluene.

***External Quantum Efficiency and light J-V*:** External Quantum Efficiency (EQE) spectra were registered after the monochromatic illumination of the photodiodes by a 250 W power Quartz Tungsten Halogen (QTH) lamp enclosed in an F/1-aperture lamp housing and coupled to a

Cornerstone 1/8 m monochromator (CS-130-USB-3-MC), capable of covering the 300-2200 nm spectral range. The optical power output of the lamp was determined based on a calibrating photodiode (818-UV/DB UV Detector, Newport DB15 Calibration Module) with known responsivity, and the EQE spectra of the devices were determined based on the device photocurrent as acquired by a source meter unit (2401 Keithley) with a detection limit of 10 pA (corresponding to 190 pA/cm^2 considering the effective area of the devices under test) and 1 μV. Photocurrent density – voltage characteristics of the PtOEP photodiodes were registered both under white light illumination and after laser photoexcitation. A Hg/Xe light source (Research F/2.2 Illumination Source 200 W Hg/Xe Ozone-free Arc Lamp, Newport) was used as the white light source, the output of which was determined based on a calibrating photodiode. For laser induced photocurrent measurements a DPSS CW 532 nm laser (MGL-III-532, CNI Optoelectronics Tech.CO. Ltd) was used. The obtained J-V curves were recorded as the output of the Hg/Xe light source and the cw laser were attenuated progressively with neutral density filters of known transmittance.

***Dark Current Characterization*:** The dark current density of all photodiodes was monitored with the acquisition of dark *J-V* curves recorded in the voltage range between -2 – 3 V when a Keithley electrometer (Source Meter Unit 2401) was used. Unipolar hole-only devices with thermally evaporated PtOEP layers were fabricated for studying charge transport properties of the PtOEP system. The device configuration of the hole-only was glass/ITO/PEDOT:PSS/PtOEP/Au. The thickness of thermally evaporated PtOEP films was determined by a Tencor P16 Stylus profiler.

Atomic force microscopy imaging: AFM imaging was performed with a Dimension Icon Bruker AFM microscope operated in a tapping mode and triangular geometry probes (Scanasyst-Air)

with tip radius between 2 – 12 nm were used. Topography mapping of the PtOEP thin films was applied on thermally evaporated PtOEP layers deposited on glass/ITO/PEDOT:PSS substrates. Image processing and statistical analysis were conducted using the Gwyddion software.

***Photoluminescence spectroscopy*:** Time-integrated photoluminescence (PL) spectra of the PtOEP films deposited on fused silica substrates were recorded at room temperature. The emitted light was dispersed in a miniature spectrograph (FLAME-S-VIS-NIR-ES) and detected with a Sony ILX511B linear silicon CCD array. During PL characterization the films were kept in a cryostat that was evacuated by a turbomolecular pump (HighCube 80 Dry Vacuum Pumping Station, Pfeiffer Vacuum) so that a dynamic vacuum of a typical pressure of 10^{-6} mbar was maintained during the measurements. Photoexcitation intensity-dependent measurements were performed by using the combination of a set of neutral density filters of known transmittance values at 532 nm and the average laser power was determined with a thermopile power sensor (PS19Q, Coherent Inc.) coupled to a FieldMaxII-TOP power/energy meter (Coherent Inc.).

***X-ray diffraction*:** The x-ray diffraction (XRD) patterns were acquired in an Ultima IV (Rigaku) diffractometer, equipped with a Cu tube (Cu Ka, λ=0.15418 nm) and operated at 40 kV and 40 mA. The x-ray beam of the instrument was configured in parallel mode by a multilayer curved mirror optics (CBO) and the patterns were acquired in conventional Bragg-Brentano scans in the 2θ range of 5^{o} – 20^{o}.

ASSOCIATED CONTENT

Supporting Information. The following file is available free of charge. UV-Vis absorption spectra of the spin-coated a-PS:PtOEP 10 wt% and the thermally evaporated PtOEP films, dark current J-V curve of hole-only PtOEP device (PDF)

AUTHOR INFORMATION

* Panagiotis E. Keivanidis, e-mail: p.keivanidis@cut.ac.cy

Notes

The authors declare no competing financial interests.

ACKNOWLEDGMENT

This work was co-funded by the European Regional Development Fund and the Republic of Cyprus through the Research and Innovation Foundation (Project: EXCELLENCE/1216/0010)

REFERENCES

1. Tang, C. W.; VanSlyke, S. A., Organic electroluminescent diodes. **1987,** *51* (12), 913-915.
2. Burroughes, J. H.; Bradley, D. D. C.; Brown, A. R.; Marks, R. N.; Mackay, K.; Friend, R. H.; Burns, P. L.; Holmes, A. B., Light-emitting diodes based on conjugated polymers. *Nature* **1990,** *347* (6293), 539-541.
3. Koezuka, H.; Tsumura, A.; Ando, T., Field-effect transistor with polythiophene thin film. *Synthetic Metals* **1987,** *18* (1), 699-704.
4. Tang, C. W., Two-layer organic photovoltaic cell. **1986,** *48* (2), 183-185.
5. Gong, X.; Tong, M.; Xia, Y.; Cai, W.; Moon, J. S.; Cao, Y.; Yu, G.; Shieh, C.-L.; Nilsson, B.; Heeger, A. J., High-Detectivity Polymer Photodetectors with Spectral Response from 300 nm to 1450 nm. **2009,** *325* (5948), 1665-1667.
6. Silinsh, E. A.; Kolesnikov, V. A.; Muzikante, I. J.; Balode, D. R., On Charge Carrier Photogeneration Mechanisms in Organic Molecular Crystals. **1982,** *113* (1), 379-393.
7. Heeger, A. J., 25th Anniversary Article: Bulk Heterojunction Solar Cells: Understanding the Mechanism of Operation. **2014,** *26* (1), 10-28.
8. Gélinas, S.; Rao, A.; Kumar, A.; Smith, S. L.; Chin, A. W.; Clark, J.; Poll, T. S. v. d.; Bazan, G. C.; Friend, R. H., Ultrafast Long-Range Charge Separation in Organic Semiconductor Photovoltaic Diodes. **2014,** *343* (6170), 512-516.
9. Gulbinas, V.; Hertel, D.; Yartsev, A.; Sundström, V., Charge carrier photogeneration and recombination in ladder-type poly(para-phenylene): Interplay between impurities and external electric field. *Physical Review B* **2007,** *76* (23), 235203.
10. Clarke, T. M.; Durrant, J. R., Charge Photogeneration in Organic Solar Cells. *Chemical Reviews* **2010,** *110* (11), 6736-6767.

11. Hahn, T.; Tscheuschner, S.; Saller, C.; Strohriegl, P.; Boregowda, P.; Mukhopadhyay, T.; Patil, S.; Neher, D.; Bässler, H.; Köhler, A., Role of Intrinsic Photogeneration in Single Layer and Bilayer Solar Cells with C60 and PCBM. *The Journal of Physical Chemistry C* **2016,** *120* (43), 25083-25091.
12. Dong, Y.; Nikolis, V. C.; Talnack, F.; Chin, Y.-C.; Benduhn, J.; Londi, G.; Kublitski, J.; Zheng, X.; Mannsfeld, S. C. B.; Spoltore, D.; Muccioli, L.; Li, J.; Blase, X.; Beljonne, D.; Kim, J.-S.; Bakulin, A. A.; D'Avino, G.; Durrant, J. R.; Vandewal, K., Orientation dependent molecular electrostatics drives efficient charge generation in homojunction organic solar cells. *Nature Communications* **2020,** *11* (1), 4617.
13. Garbugli, M.; Gambetta, A.; Schrader, S.; Virgili, T.; Lanzani, G., Multi-photon non-linear photocurrent in organic photodiodes. *Journal of Materials Chemistry* **2009,** *19* (40), 7551-7560.
14. Baeg, K.-J.; Binda, M.; Natali, D.; Caironi, M.; Noh, Y.-Y., Organic Light Detectors: Photodiodes and Phototransistors. **2013,** *25* (31), 4267-4295.
15. Jansen-van Vuuren, R. D.; Armin, A.; Pandey, A. K.; Burn, P. L.; Meredith, P., Organic Photodiodes: The Future of Full Color Detection and Image Sensing. **2016,** *28* (24), 4766-4802.
16. Yang, D.; Ma, D., Development of Organic Semiconductor Photodetectors: From Mechanism to Applications. **2019,** *7* (1), 1800522.
17. Ren, H.; Chen, J.-D.; Li, Y.-Q.; Tang, J.-X., Recent Progress in Organic Photodetectors and their Applications. **2021,** *8* (1), 2002418.
18. Jansen-van Vuuren, R. D.; Armin, A.; Pandey, A. K.; Burn, P. L.; Meredith, P., Organic Photodiodes: The Future of Full Color Detection and Image Sensing. *Advanced Materials* **2016,** *28* (24), 4766-4802.
19. Gong, X.; Tong, M.; Xia, Y.; Cai, W.; Moon, J. S.; Cao, Y.; Yu, G.; Shieh, C. L.; Nilsson, B.; Heeger, A. J., High-detectivity polymer photodetectors with spectral response from 300 nm to 1450 nm. *Science* **2009,** *325* (5948), 1665-7.
20. Bristow, H.; Jacoutot, P.; Scaccabarozzi, A. D.; Babics, M.; Moser, M.; Wadsworth, A.; Anthopoulos, T. D.; Bakulin, A.; McCulloch, I.; Gasparini, N., Nonfullerene-Based Organic Photodetectors for Ultrahigh Sensitivity Visible Light Detection. *ACS Applied Materials & Interfaces* **2020,** *12* (43), 48836-48844.
21. Kim, I. K.; Jo, J. H.; Lee, J.; Choi, Y. J., Detectivity analysis for organic photodetectors. *Organic Electronics* **2018,** *57*, 89-92.
22. Ramuz, M.; Bürgi, L.; Winnewisser, C.; Seitz, P., High sensitivity organic photodiodes with low dark currents and increased lifetimes. *Organic Electronics* **2008,** *9* (3), 369-376.
23. Georgiadou, D. G.; Lin, Y.-H.; Lim, J.; Ratnasingham, S.; McLachlan, M. A.; Snaith, H. J.; Anthopoulos, T. D., High Responsivity and Response Speed Single-Layer Mixed-Cation Lead Mixed-Halide Perovskite Photodetectors Based on Nanogap Electrodes Manufactured on Large-Area Rigid and Flexible Substrates. *Advanced Functional Materials* **2019,** *29* (28), 1901371.
24. Lee, K.-H.; Leem, D.-S.; Castrucci, J. S.; Park, K.-B.; Bulliard, X.; Kim, K.-S.; Jin, Y. W.; Lee, S.; Bender, T. P.; Park, S. Y., Green-Sensitive Organic Photodetectors with High Sensitivity and Spectral Selectivity Using Subphthalocyanine Derivatives. *ACS Applied Materials & Interfaces* **2013,** *5* (24), 13089-13095.
25. Tedde, S. F.; Kern, J.; Sterzl, T.; Fürst, J.; Lugli, P.; Hayden, O., Fully Spray Coated Organic Photodiodes. *Nano Letters* **2009,** *9* (3), 980-983.
26. Canjeevaram Balasubramanyam, R. K.; Kandjani, A. E.; Harrison, C. J.; Abdul Haroon Rashid, S. S. A.; Sabri, Y. M.; Bhargava, S. K.; Narayan, R.; Basak, P.; Ippolito, S. J., 1,4-

Dihydropyrrolo[3,2-b]pyrroles as a Single Component Photoactive Layer: A New Paradigm for Broadband Detection. *ACS Applied Materials & Interfaces* **2017,** *9* (33), 27875-27882.
27. Clark, J.; Lanzani, G., Organic photonics for communications. *Nature Photonics* **2010,** *4* (7), 438-446.
28. Fron, E.; Schweitzer, G.; Jacob , J.; Van Vooren, A.; Beljonne, D.; Müllen, K.; Hofkens, J.; Van der Auweraer, M.; De Schryver, F. C., Singlet–Singlet Annihilation Leading to a Charge-Transfer Intermediate in Chromophore-End-Capped Pentaphenylenes. *ChemPhysChem* **2007,** *8* (9), 1386-1393.
29. Scheblykin, I. G.; Yartsev, A.; Pullerits, T.; Gulbinas, V.; Sundström, V., Excited State and Charge Photogeneration Dynamics in Conjugated Polymers. *The Journal of Physical Chemistry B* **2007,** *111* (23), 6303-6321.
30. Gehrig, D. W.; Howard, I. A.; Laquai, F., Charge Carrier Generation Followed by Triplet State Formation, Annihilation, and Carrier Recreation in PBDTTT-C/PC60BM Photovoltaic Blends. *The Journal of Physical Chemistry C* **2015,** *119* (24), 13509-13515.
31. Baldo, M. A.; O'Brien, D. F.; You, Y.; Shoustikov, A.; Sibley, S.; Thompson, M. E.; Forrest, S. R., Highly efficient phosphorescent emission from organic electroluminescent devices. *Nature* **1998,** *395* (6698), 151-154.
32. Bansal, A. K.; Holzer, W.; Penzkofer, A.; Tsuboi, T., Absorption and emission spectroscopic characterization of platinum-octaethyl-porphyrin (PtOEP). *Chemical Physics* **2006,** *330* (1), 118-129.
33. Nifiatis, F.; Su, W.; Haley, J. E.; Slagle, J. E.; Cooper, T. M., Comparison of the Photophysical Properties of a Planar, PtOEP, and a Nonplanar, PtOETPP, Porphyrin in Solution and Doped Films. *The Journal of Physical Chemistry A* **2011,** *115* (47), 13764-13772.
34. Tsuboi, T.; Tanigawa, M.; Kawami, S.; Tsuji, T., Organic LED device based on PtOEP phosphor without doping in host material. *Current Applied Physics* **2005,** *5* (6), 633-639.
35. Yang, X.-H.; Jaiser, F.; Neher, D., Physical Processes in Polymer-Based Electrophosphorescent Devices. In *Highly Efficient OLEDs with Phosphorescent Materials*, **2007**, pp 221-258.
36. Keivanidis, P. E.; Baluschev, S.; Miteva, T.; Nelles, G.; Scherf, U.; Yasuda, A.; Wegner, G., Up-conversion photoluminescence in polyfluorene doped with metal (II)-octaethyl porphyrins. *Adv. Mater.* **2003,** *15* (24), 2095-+.
37. Keivanidis, P. E.; Baluschev, S.; Lieser, G.; Wegner, G., Inherent Photon Energy Recycling Effects in the Up-Converted Delayed Luminescence Dynamics of Poly(fluorene)–PtIIoctaethyl Porphyrin Blends. *ChemPhysChem* **2009,** *10* (13), 2316-2326.
38. Baluschev, S.; Keivanidis, P. E.; Wegner, G.; Jacob, J.; Grimsdale, A. C.; Müllen, K.; Miteva, T.; Yasuda, A.; Nelles, G., Upconversion Photoluminescence in Poly(ladder-type-Pentaphenylene) Doped with Metal (II)-Octaethyl Porphyrins. *Appl. Phys. Lett.* **2005,** *86* (6), 061904.
39. Keivanidis, P. E.; Laquai, F.; Robertson, J. W. F.; Baluschev, S.; Jacob, J.; Müllen, K.; Wegner, G., Electron-Exchange-Assisted Photon Energy Up-Conversion in Thin Films of pi-Conjugated Polymeric Composites. *J. Phys. Chem. Lett.* **2011,** *2* (15), 1893-1899.
40. Goudarzi, H.; Limbu, S.; Cabanillas-González, J.; Zenonos, V. M.; Kim, J.-S.; Keivanidis, P. E., Impact of molecular conformation on triplet-fusion induced photon energy up-conversion in the absence of exothermic triplet energy transfer. *Journal of Materials Chemistry C* **2019,** *7* (12), 3634-3643.

41. Noh, Y.-Y.; Kim, J.-J.; Yoshida, Y.; Yase, K., Effect of Molecular Orientation of Epitaxially Grown Platinum(II) Octaethyl Porphyrin Films on the Performance of Field-Effect Transistors. *Advanced Materials* **2003,** *15* (9), 699-702.
42. Savenije, T. J.; Goossens, A., Hole transport in porphyrin thin films. *Physical Review B* **2001,** *64* (11), 115323.
43. Campione, M.; Fumagalli, E.; Raimondo, L.; Monguzzi, A.; Meinardi, F.; Sassella, A., Control of pi-pi Interactions in Epitaxial Films of Platinum(II) Octaethyl Porphyrin. *Chem. Matter.* **2011,** *23*, 832-840.
44. Perez, M. D.; Borek, C.; Djurovich, P. I.; Mayo, E. I.; Lunt, R. R.; Forrest, S. R.; Thompson, M. E., Organic Photovoltaics Using Tetraphenylbenzoporphyrin Complexes as Donor Layers. *Advanced Materials* **2009,** *21* (14-15), 1517-1520.
45. Kalinowski, J.; Stampor, W.; Szmytkowski, J.; Cocchi, M.; Virgili, D.; Fattori, V.; Marco, P. D., Photophysics of an electrophosphorescent platinum (II) porphyrin in solid films. *The Journal of Chemical Physics* **2005,** *122* (15), 154710.
46. M Dongol, M. M. E.-N., A El-Denglawey, A A Abuelwafa, T Soga, Alternating current characterization of nano-Pt(II) octaethylporphyrin (PtOEP) thin film as a new organic semiconductor. *Chin. Phys. B* **2016,** *25* (6), 67201-067201.
47. Borders, B.; Adinehnia, M.; Rosenkrantz, N.; Zijll, M. v.; Hipps, K. W.; Mazur, U., Photoconductive behavior of binary porphyrin crystalline assemblies. *Journal of Porphyrins and Phthalocyanines* **2017,** *21* (09), 569-580.
48. Che, C.-M.; Xiang, H.-F.; Chui, S. S.-Y.; Xu, Z.-X.; Roy, V. A. L.; Yan, J. J.; Fu, W.-F.; Lai, P. T.; Williams, I. D., A High-Performance Organic Field-Effect Transistor Based on Platinum(II) Porphyrin: Peripheral Substituents on Porphyrin Ligand Significantly Affect Film Structure and Charge Mobility. *Chemistry – An Asian Journal* **2008,** *3* (7), 1092-1103.
49. Milgrom, L. R.; Sheppard, R. N.; Slawin, A. M. Z.; Williams, D. J., X-ray crystal structure of 2,3,7,8,12,13,17,18-octaethylporphyrinatoplatinum(II) (PtOEP): Potential for correlation of meso-carbon bond-angle (Ĉm) With one-bond 13Cmeso□1Hmethine coupling constant in some diamagnetic metal complexes of OEP. *Polyhedron* **1988,** *7* (1), 57-61.
50. Dienel, T.; Proehl, H.; Fritz, T.; Leo, K., Novel near-infrared photoluminescence from platinum(II)-porphyrin (PtOEP) aggregates. *Journal of Luminescence* **2004,** *110* (4), 253-257.
51. Bell, T. D. M.; Jacob, J.; Angeles-Izquierdo, M.; Fron, E.; Nolde, F.; Hofkens, J.; Müllen, K.; Schryver, F. C. D., Charge transfer enhanced annihilation leading to deterministic single photon emission in rigid perylene end-capped polyphenylenes. *Chemical Communications* **2005,** (39), 4973-4975.
52. Mężyk, J.; Kalinowski, J.; Meinardi, F.; Tubino, R., Triplet exciton interactions in solid films of an electrophosphorescent Pt (II) porphyrin. *Applied Physics Letters* **2005,** *86* (11), 111916.
53. Lin, Y. L.; Koch, M.; Brigeman, A. N.; Freeman, D. M. E.; Zhao, L.; Bronstein, H.; Giebink, N. C.; Scholes, G. D.; Rand, B. P., Enhanced sub-bandgap efficiency of a solid-state organic intermediate band solar cell using triplet–triplet annihilation. *Energy & Environmental Science* **2017,** *10* (6), 1465-1475.
54. Koster, L. J. A.; Mihailetchi, V. D.; Ramaker, R.; Blom, P. W. M., Light intensity dependence of open-circuit voltage of polymer:fullerene solar cells. *Applied Physics Letters* **2005,** *86* (12), 123509.
55. Proctor, C. M.; Kuik, M.; Nguyen, T.-Q., Charge carrier recombination in organic solar cells. *Progress in Polymer Science* **2013,** *38* (12), 1941-1960.

SUPPORTING INFORMATION

Low-Power Non-linear Photocurrent Generation via Excited State Fusion in Single-component Nanostructured Organic Photodetectors

Giannis Antoniou [a)], Peisen Yuan [a)], Loukas Koutsokeras [a)], Stavros Athanassopoulos [b)], Daniele Fazzi [c)], Julianna Panidi [d)], Dimitra G. Georgiadou [d)], Themis Prodromakis [d)], Panagiotis E. Keivanidis [a)]*

a) Device Technology and Chemical Physics Laboratory, Department of Mechanical Engineering and Materials Science and Engineering, Cyprus University of Technology, 45 Kitiou Kyprianou str., Limassol 3041, Cyprus

b) Departamento de Fisica, Universidad Carlos III de Madrid, Spain

c) Dipartimento di Chimica "Giacomo Ciamician", Università di Bologna, via F. Selmi 2, 40126, Bologna (Italy)

d) Centre for Electronics Frontiers, Electronics and Computer Science, University of Southampton, Highfield Campus, University Road, Building 53 (Mountbatten), Southampton SO17 1BJ, United Kingdom

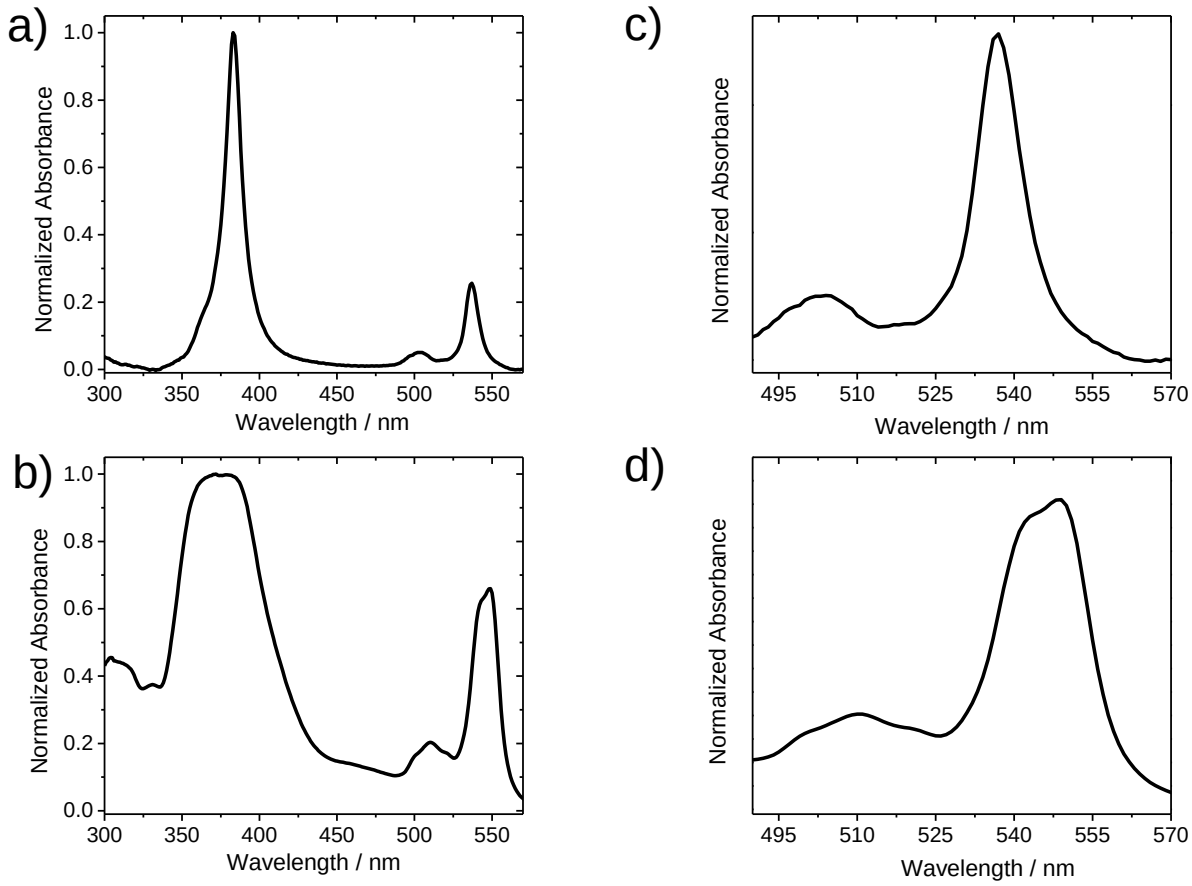

Figure S1. Normalized absorption spectra of a) a-PS:PtOEP 10 wt% film developed by spin-coating of a toluene solution, b) thermally evaporated PtOEP film. Selected spectral ranges of (a) and (b) that present the normalized Q-band absorption spectra of c) a-PS:PtOEP 10 wt% film developed by spin-coating of a toluene solution and d) thermally evaporated PtOEP film.

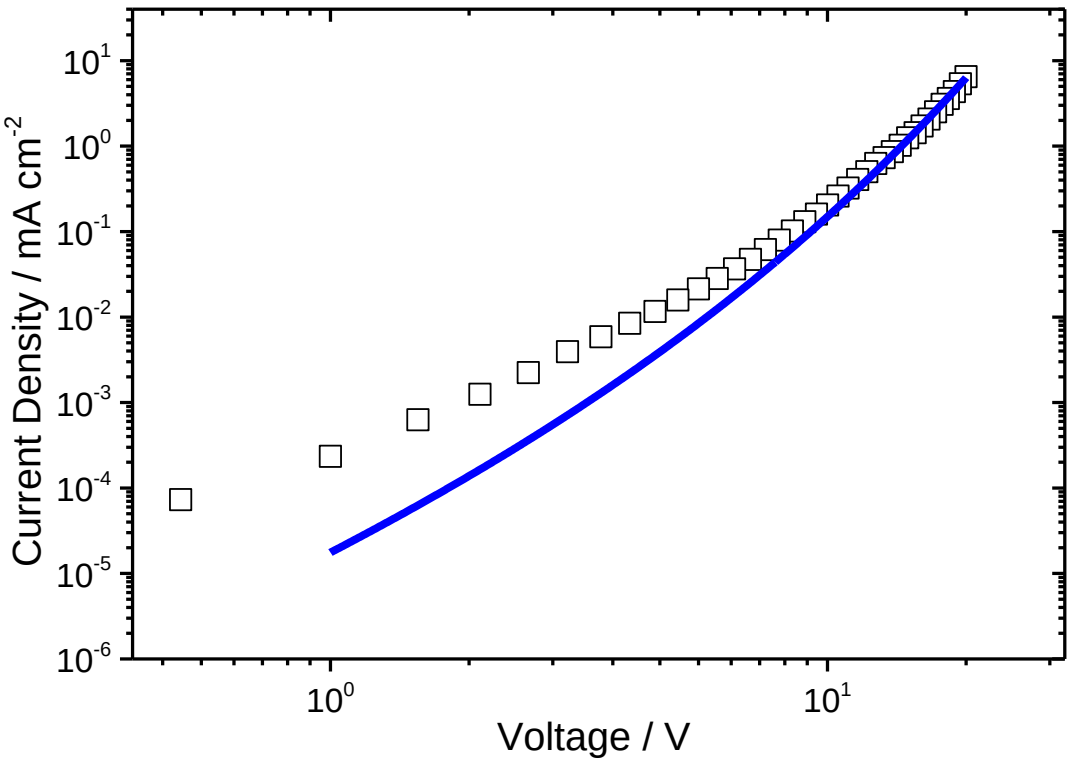

Figure S2. Dark J-V curves of a hole-only PtOEP device with the ITO/PEDOT:PSS/active layer/Au configuration. The solid line is fit to the data according to Eq. 1

$$J(V) = \frac{9}{8}\varepsilon_0\varepsilon_r\mu_0\frac{V^2}{L^3}\,e^{0.89\beta\sqrt{\frac{V}{L}}} \qquad \text{Eq. 1}$$

Equation 1 corresponds to a modified Mott-Gurney equation, by considering the Poole Frenkel effect [1], where ε_0 and ε correspond to the vacuum permittivity and the material dielectric constant respectively, μ_0 is the zero-field hole mobility, V corresponds to the applied voltage and L corresponds to the active layer thickness.

REFERENCES.

1. F. Machui, S. Rathgeber, N. Li, T. Ameri, C. J. Brabec, Influence of a ternary donor material on the morphology of a P3HT:PCBM blend for organic photovoltaic devices *J. Mater. Chem.*, **2012**, 22, 15570-15577